Type I interferon modulates Langerhans cell ADAM17 to promote photosensitivity in lupus

Thomas M. Li[1], Keila R. Veiga[1,2,†], Noa Schwartz[1,3,††], Yurii Chinenov[4], David J. Oliver[4], Jose Lora[5,6], Ali Jabbari[7,†††], Yong Liu[8], William D. Shipman[1,9,††††], Marvin J. Sandoval[1], Isabel F. Sollohub[1], William G. Ambler[1,2], Mehdi Rashighi[10], James G. Krueger[7], Niroshana Anandasabapathy[8,11], Carl P. Blobel[5,6,12], Theresa T. Lu[1,2,3,11,13,*]

[1]Autoimmunity and Inflammation Program, Hospital for Special Surgery, New York, NY 10021
[2]Pediatric Rheumatology, Department of Medicine, Hospital for Special Surgery, New York, NY 10021
[3]Rheumatology, Department of Medicine, Hospital for Special Surgery, New York, NY 10021
[4]David Z. Rosensweig Genomics Research Center, Hospital for Special Surgery, New York, NY 10021
[5]Arthritis and Tissue Degeneration Program, Hospital for Special Surgery, New York, NY 10021
[6]Department of Physiology, Biophysics, and Systems Biology, Weill Cornell Medicine, New York, NY, 10065
[7]Laboratory of Investigative Dermatology, Rockefeller University, New York, NY 10065
[8]Department of Dermatology, Weill Cornell Medical College, New York, NY 10065
[9]Weill Cornell Tri-Institutional MD-PhD Program, New York, NY 10065
[10]Department of Dermatology, University of Massachusetts Medical School, Worcester, MA 01655
[11]Immunology and Microbial Pathogenesis Program, Weill Cornell Graduate School of Medical Sciences, New York, NY 10065
[12]Institute for Advanced Study, Technische Universität München, D-85748 Garching, Germany
[13]Department of Microbiology and Immunology, Weill Cornell Medicine, New York, NY 10065

[†]K. R. Veiga's current address is Department of Rheumatology, Maria Fareri Children's Hospital, Valhalla, New York 10595
[††]N. Schwartz's current address is Department of Medicine (Rheumatology), Montefiore Medical Center/Albert Einstein College of Medicine, Bronx, NY 10647
[†††]A. Jabbari's current address is Department of Dermatology, University of Iowa Hospital and Clinics, Iowa City, IA 52242
[††††]W. D. Shipman's current address is Department of Dermatology, Yale-New Haven Hospital, New Haven, CT 06510

*Corresponding author: Theresa T. Lu MD, PhD
Hospital for Special Surgery
535 East 70 Street
New York, NY 10021
Tel: (212) 774-2532
Email: LuT@HSS.edu

ABSTRACT

Type I IFN (IFN-I) mediates autoimmune and inflammatory conditions, and better understanding IFN-I-driven pathogenesis could expand therapeutic possibilities. Lupus is an autoimmune disease characterized by photosensitivity, inflammatory skin lesions, and systemic organ damage. Patients have an IFN-I signature in blood and tissues and anifrolumab (anti-IFNAR1), developed for lupus and recently FDA-approved, underscores the importance of IFN-I in pathogenesis. Anifrolumab is especially efficacious for cutaneous disease, but mechanisms are poorly understood. Langerhans cells (LCs) normally limit UVR-induced skin injury via ADAM17, a metalloprotease that clips from the cell membrane and activates skin-protective EGFR ligands. Downregulation of LC ADAM17 mRNA and activity in lupus models contributes to photosensitivity, and here we link IFN-I pathogenesis with LC dysfunction. We show that murine model and human lupus non-lesional skin have IFN-I signatures and that IFN-I reduces ADAM17 sheddase activity in LCs. Furthermore, anti-IFNAR1 in multiple murine lupus models restores LC ADAM17 function and reduces photosensitivity in an EGFR and LC ADAM17-dependent manner. These results suggest that IFN-I contributes to photosensitivity in lupus by downregulating LC ADAM17 function, providing mechanisms for IFN-I pathogenesis and anifrolumab efficacy and highlighting the importance of LCs as a potential therapeutic target.

INTRODUCTION

Type I IFN (IFN-I), best known for its roles in host defense, is becoming better appreciated as a pathogenic mediator of autoimmune and inflammatory disease (Crow, 2014; Rodero and Crow, 2016; Snell et al., 2017). Yet the mechanisms by which IFN-I contributes to disease remain incompletely understood. The autoimmune disease lupus is an IFN-I-associated disease that can manifest as cutaneous disease (cutaneous lupus erythematosus (CLE)) alone or as part of the systemic form of the disease (systemic lupus erythematosus (SLE)). A prominent IFN-I signature is found in circulating cells and tissues (Baechler et al., 2003; Bennett et al., 2003; Crow and Ronnblom, 2019; Der et al., 2017; Der et al., 2019; Jabbari et al., 2014; Kahlenberg, 2021; Kirou et al., 2004) and the development and recent FDA approval of anifrolumab (anti-IFNAR1) for SLE highlights the importance of IFN-I as a mediator of disease. As such, understanding how IFN-I contributes to lupus pathogenesis could provide insight into the mechanisms of IFN-I-mediated pathology in this and other immune diseases (Boukhaled et al., 2021; Crow and Ronnblom, 2019; Roy et al., 2020).

Photosensitivity, an abnormal sensitivity of the skin to ultraviolet radiation (UVR), is considered to be a major contributor to CLE inflammatory lesion development and can also trigger flares of systemic disease in SLE (Patel et al., 2020; Sim et al., 2021). Recent evidence has pointed to a role for IFN-I in photosensitivity. First, an IFN-I signature is detected in lesional as well as non-lesional skin tissue (Der et al., 2017; Der et al., 2019; Kahlenberg, 2021; Lambers et al., 2019), suggesting that even non-lesional skin cells are chronically exposed to high levels of IFN-I that can sensitize the tissue for disease-related injury. Supportive of this idea is that IFN-I can prime keratinocytes for UVR-induced apoptosis (Tsoi et al., 2019). Second, IFNAR1-deficiency in the MRL-*Fas*^{lpr} (MRL/lpr) lupus model abrogated spontaneous skin

lesion development (Nickerson et al., 2013). Third, although anifrolumab was found to reduce a global disease score in SLE, the treatment was most consistently associated with reduction in the skin score, a measure of CLE (Furie et al., 2017; Morand et al., 2020). Better understanding lupus pathogenesis, then, would be aided by understanding the mechanisms by which IFN-I contributes to photosensitivity.

We recently reported that Langerhans cells (LCs) can limit UVR-induced keratinocyte apoptosis by expressing a disintegrin and metalloprotease 17 (ADAM17) which releases membrane-bound epidermal growth factor receptor (EGFR) ligands that then promote keratinocyte survival via EGFR (Shipman et al., 2018). Two distinct photosensitive lupus mouse models showed low LC *Adam17* mRNA which corresponded to reduced LC ADAM17 sheddase activity, and photosensitivity could be reduced by topical EGFR ligand application, suggesting that the lack of LC ADAM17 shedding activity contributes to photosensitivity. Non-lesional skin of lupus nephritis patients showed reduced epidermal EGFR phosphorylation, further supporting that LC dysfunction contributes to photosensitivity in lupus. The drivers of LC dysfunction remain unknown.

Here, we test the hypothesis that the elevated IFN-I in the lupus tissue environment mediates LC ADAM17 dysregulation to contribute to photosensitivity, and, as a corollary, anti-IFNAR1 reduces photosensitivity by rescuing LC ADAM17 activity. We show that non-lesional skin from CLE patients and lupus mouse models share an IFN-I signature and that IFN-I downregulates LC ADAM17 sheddase activity *ex vivo* and *in vivo*. In multiple lupus models, anti-IFNAR1 restores LC ADAM17 activity and reduces photosensitivity in an EGFR and LC ADAM17-dependent manner. These results provide a mechanism by which IFN-I contributes to photosensitivity in lupus and by which anti-IFNAR1 therapies function, further support a central

role for LC dysfunction in lupus pathogenesis, and provide insight into IFN-I-mediated pathogenesis in IFN-I-associated autoimmune and inflammatory states.

RESULTS

Non-lesional skin in human and murine models of lupus share an interferon (IFN) signature

We assessed gene expression signatures in non-lesional skin of CLE patients and two distinct lupus mouse models to better understand the extent to which an IFN-I signature was common to non-lesional skin in both human and murine lupus settings. Non-lesional skin from a CLE cohort whose lesional skin was previously shown to express upregulated IFN signature (Jabbari et al., 2014) exhibited a significantly different expression profile compared to that of healthy controls by microarray analysis (Figure S1A; Table S1). Differential pathway analysis via Quantitative Set Analysis for Gene Expression (QuSAGE) showed that an IFN-I-related pathway was among the most upregulated in CLE non-lesional skin (Figure 1A). The IFN-I pathway was comprised of several upregulated IFN-stimulated transcription factors, including IRF 1,2,7,8 and 9 along with multiple IRF targets (ISG15, IFIT1, IFIT3, MX1, MX2) (Figure 1 B, C, and S1B). Consistent with potential roles for IFNγ in lupus (Jenks et al., 2018), an IFNγ-related pathway was also among the most upregulated (Figure 1A). This cohort of CLE patients included one SLE patient (Jabbari et al., 2014) and the upregulated IFN-I signature in their non-lesional skin echoed the IFN-I signature found in non-lesional keratinocytes of SLE patients (Der et al., 2017; Der et al., 2019), suggesting that IFN-I upregulation in non-lesional skin is a common characteristic across CLE and SLE.

The CLE non-lesional skin microarray data also echoed the idea of reduced LC ADAM17 activity that was suggested by tissue imaging of SLE patients (Shipman et al., 2018). *CD207* mRNA (Langerin) was downregulated in CLE skin (Figure 1B), potentially reflecting the reduced LC numbers in SLE non-lesional skin (Shipman et al., 2018) or reduced CD207

expression by LCs. Further supporting the idea of LC ADAM17 dysfunction and subsequent reduced epidermal EGFR signaling was the reduction in CLE skin of the EGFR-associated MAP kinase inactivation of SMRT corepressor pathway (BIOCARTA_EGFR_SMRTE_PATHWAY, Figure 1A, Table S2).

We examined for IFN-I signatures in non-lesional skin of two photosensitive murine lupus models. The MRL-*Fas*^{lpr} (MRL/lpr) model, with the *lpr* mutation in the *Fas* gene, has reduced LC *Adam17* mRNA and LC ADAM17 sheddase and skin-protective functions (Shipman et al., 2018). Although the differences in gene expression between MRL/lpr mice and the parental MRL-MpJ (MRL/+) strain by RNA sequencing were less dramatic than those in the human cohort (Figures 1A-C and 1D-F) (Table S3), differential pathway analysis showed that the IFN-α/β-related pathway was among the most highly expressed in MRL/lpr mice (Figure 1D) (Table S4). An IFN-γ pathway was similarly upregulated, and, consistent with the activation of IFN pathways, several IRF transcription factors and their targets were expressed at higher levels in MRL/lpr mice (Figure 1E, F, and Figure S1C).

As an alternative analysis, we performed ranked Gene Set Enrichment Analysis (GSEA) separately for human and murine datasets using negative log-transformed p values as a ranking variable, constructed pathway similarity networks, and compared selected pathways (FDR<0.005) in CLE patients and MRL/lpr mice. Consistent with QuSAGE analysis (Figure 1A and D), IFN-related pathways were enriched in human non-lesional skin and the MRL/lpr lupus model (Figure 1G), along with several other pathways often associated with SLE (Fig 1G): T helper pathway (nodule 26); natural killer cell-mediated cytotoxicity (nodule 28); Toll-like receptor pathways (nodules 36,46); JAK-STAT signaling pathway (nodule 43); and multiple pathways associated with complement activation (nodules 6, 23, 29, 34, 52, 53, 58, 61, 62, 64,

75, 88, 94, 95). For the full list of pathways identified by ranked GSEA, see Table S5. Direct comparison of differentially expressed genes in MRL/lpr mouse and CLE non-lesional skin (Figure 1H) revealed a gene signature typical of nucleic acid-driven interferonopathies dominated by IFN-stimulated transcription factors (IRF1,3,9 and STAT1), IFN-induced viral restriction factors (BST2, SAMHD1, DDX60, IFIH1, ZBP1), neutrophilic markers (HMOX1, S100A8, S100A9, LCN2, RSAD2), and apoptosis-related genes (XAF1, TNFSF10). Interestingly, several keratins (KRT16, 6B and 34) were expressed at high levels in MRL/lpr and CLE non-lesional skin, which are known to be rapidly induced in response to skin damage and, in turn, downregulate skin inflammatory response (Lessard et al., 2013). These data suggest that epidermal homeostasis is disturbed in even non-lesional skin and is consistent with the idea that this tissue is primed for photosensitive responses.

The B6.Sle1yaa model is driven by the Sle1 lupus susceptibility locus derived from the lupus-prone NZB2410 mice in combination with the Y chromosome autoimmune accelerator locus whose effects are attributed to *Tlr7* duplication (Pisitkun et al., 2006; Subramanian et al., 2006). These mice are photosensitive and have reduced LC *Adam17* mRNA expression (Shipman et al., 2018). B6.Sle1yaa mice expression of several genes from the Yaa locus including Tlr7 was elevated (Figure S1E) compared to the parental B6 strain. Although the differences in B6 and B6.Sle1yaa transcriptomes at the young age assayed are modest (Table S6), TLR7 is a driver of IFN-I, and several genes involved in regulation of and response to IFN were expressed at higher levels, including Irf7, Irf9, Isg15, Xaf1, Selp, and Ube2l6 (Figure S1F). Interestingly, although LC numbers were not different at 10 months of age when this model is fully diseased (Shipman et al., 2018), *Cd207* expression in the young mice examined here is downregulated when compared to B6 controls (Figure S1F), similar to the findings in CLE skin

(Figure 1B). Both the MRL/lpr and B6.Sle1yaa lupus models, then, are similar to human lupus patients in showing increased IFN-stimulated gene expression in non-lesional skin. Together, the data suggest that the skin in both human and murine models of lupus are exposed to a high IFN-I environment and are consistent with the possibility that IFN-I could contribute to LC ADAM17 dysfunction.

IFN-I is sufficient to downregulate ADAM17 activity on murine and human LCs

We asked whether IFN-I could alter ADAM17 sheddase activity or expression in wildtype LCs. We had previously measured LC ADAM17 activity in isolated LCs by assessing UVR-induced shedding of the ADAM17 substrate TNFR1 (Shipman et al., 2018). Assessing LC ADAM17 activity within a mixture of epidermal cells yielded similar results, with UVR inducing cell surface TNFR1 reduction in wildtype but not ADAM17-deficient LCs (Figure S2A-B). Incubation of the epidermal cells with IFN-κ, an IFN-I expressed highly by lupus keratinocytes (Tsoi et al., 2019), reduced LC ADAM17 activity by nearly 40% (Figure 2A) with only a 9% reduction in ADAM17 cell surface levels (Figure 2B) (Lora et al., 2021). Cell viability was not affected (Figure 2C). The IFN-κ-driven inhibition of ADAM17 activity was abrogated by the JAK1/3 inhibitor tofacitinib without altering ADAM17 protein levels (Figure 2D-E) or cell viability (Figure 2F), supporting an IFNAR-mediated inhibition of LC ADAM17 sheddase activity. Application of IFN-κ to the skin of wildtype mice reduced LC ADAM17 activity by 57% (Figure 2G) while cell surface ADAM17 was reduced by 9% (Figure 2H). Together, these data indicated that IFN-I primarily regulates murine LC ADAM17 at the level of sheddase activity *ex vivo* and *in vivo.*

We also asked about the effects of IFN-I on human LCs. While LCs can be obtained from skin biopsies or discarded tissues associated with surgical procedures, these tissues usually require lengthy enzymatic digestion to dissociate the cells (Shipman et al., 2018) whose functions may be altered during processing. We found that suction blistering yielded epidermal roofs that could be digested for a minimal amount of time to obtain an epidermal cell mixture with LCs (Figure S3) (Strassner et al., 2017). Addition of IFN-I to the epidermal cells reduced LC ADAM17 activity by 62% without altering ADAM17 expression or LC viability (Figure 2I-K). These results together showed that IFN-I can inhibit LC ADAM17 activity in both murine and human LCs and supported the idea that the high levels of IFN-I signaling could potentially contribute to LC ADAM17 dysfunction in SLE patient and murine model skin.

IFN-I is an important mediator of LC ADAM17 dysfunction in murine lupus models

The sufficiency of IFN-I in inducing LC ADAM17 dysfunction led us to ask whether the high IFN-I in lupus models contributed to LC ADAM17 dysfunction. Consistent with previous findings (Shipman et al., 2018), MRL/lpr mice showed a 42% reduction in LC ADAM17 sheddase activity when compared to control MRL/+ mice (Figure 3A). LC ADAM17 protein levels, however, were less affected, showing a 21% reduction (Figure 3B). Anti-IFNAR1 treatment at 500 μg/dose restored LC ADAM17 activity in MRL/lpr mice (Figure 3A) without increasing ADAM17 protein expression (Figure 3B). A lower dose of anti-IFNAR1 at 125 μg/dose had similar effects in rescuing LC ADAM17 sheddase function (Figure 3C-D). These results together suggested that, while not critical for modulating LC ADAM17 expression levels, IFN-I is important in inhibiting LC ADAM17 sheddase activity in MRL/lpr mice.

LCs from the B6.Sle1yaa model showed a 83% reduction in ADAM17 activity when compared to age-matched wildtype mice without similar change in ADAM17 protein levels (Figure 3E-F). Similar to MRL/lpr mice, anti-IFNAR1 restored LC ADAM17 activity in B6.Sle1yaa mice without affecting ADAM17 protein expression (Figure 3E-F). Our results across both MRL/lpr and B6.Sle1yaa lupus models suggested a scenario whereby the elevated IFN-I environment in the skin caused LC ADAM17 sheddase dysfunction.

Anti-IFNAR1 reduces photosensitivity in lupus models

We asked whether the anti-IFNAR1-driven restoration of LC ADAM17 function in the MRL/lpr mice also reduced their photosensitive response to UVR (Figure 4A). LC ADAM17 deficiency results in increased UVR-induced epidermal permeability, monocyte infiltration (Shipman et al., 2018), and ear swelling (Figure S2C), and we examined the effects of anti-IFNAR on these parameters in MRL/lpr mice. Anti-IFNAR1 treatment at 500 μg/dose reduced ear swelling in MRL/lpr mice (Figure 4B) but did not reduce epidermal permeability or cellular infiltration (Figure 4C-E). Furthermore, in control MRL/+ mice, the 500 μg anti-IFNAR1 dose actually increased UVR-induced ear swelling and epidermal permeability (Figure 4B-C), suggesting that anti-IFNAR1 increased aspects of photosensitivity in the non-lupus mice. These results echoed findings that IFNAR1 deficiency in non-lupus wildtype mice induced photosensitivity (Sontheimer et al., 2017) and reduced skin wound re-epithelization (Gregorio et al., 2010), suggesting that the 500ug anti-IFNAR1 dose was disrupting intrinsic skin functions and potentially obscuring the effects of LC ADAM17 activity restoration. We thus reduced the anti-IFNAR1 dose to 125 μg/dose, which was sufficient to restore LC ADAM17 activity in MRL/lpr mice (Figure 3C). The lower anti-IFNAR1 dose in MRL/lpr mice reduced UVR-

induced skin swelling, epidermal permeability, and monocyte and T cell accumulation (Figure 4F-I). Notably, although the lower anti-IFNAR1 dose continued to increase UVR-induced ear swelling in control MLR/+ mice (Figure 4F), it did not worsen epidermal permeability (Figure 4G), suggesting less effect on intrinsic skin functions. With the 125 μg/dose, MRL/lpr mice showed reduced epidermal permeability and monocyte and T cell accumulation in addition to reduced ear swelling compared to control antibody-treated MRL/lpr mice (Figures F-I). At 125 μg/dose, then, anti-IFNAR1 was able to both rescue LC ADAM17 function and reduce photosensitivity in MRL/lpr mice.

EGFR function and LC ADAM17 are required for the ameliorative effects of anti-IFNAR1 on photosensitivity

We sought to understand the extent to which the anti-IFNAR1-driven reduction in photosensitivity reflected the rescue of LC ADAM17 activity. As LC ADAM17 limits photosensitivity by stimulating EGFR signaling (Shipman et al., 2018), we blocked EGFR activity upon anti-IFNAR1 treatment of MRL/lpr mice (Figure 5A). The EGFR blockade abrogated the anti-IFNAR1-driven reduction in ear swelling and epidermal permeability (Figure 5B-C), suggesting that the anti-IFNAR1 requires EGFR and thus LC ADAM17 activity to ameliorate photosensitivity in MRL/lpr mice.

We directly examined the importance of LC ADAM17 in anti-IFNAR1-driven effects on photosensitivity by inducing a lupus phenotype in LC ADAM17-deficient and control mice. The imiquimod (IMQ) lupus model is induced by 5-6 weeks of topical IMQ application, resulting in autoantibodies, splenomegaly, and nephritis characteristic of human SLE and murine SLE

models (Goel et al., 2020; Yokogawa et al., 2014). Similar to MRL/lpr and B6.Sle1yaa models, IMQ-treated wildtype mice showed reduced LC ADAM17 sheddase activity in non-lesional skin without altering cell surface ADAM17 protein levels (Figure 5D-F). Interestingly, LC numbers in the skin were reduced by 35% (Figure 5G), echoing findings in human skin (Shipman et al., 2018). Anti-IFNAR1 partially restored LC ADAM17 activity without increasing protein levels (Figure 5E-F) and reduced UVR-induced swelling and epidermal permeability of IMQ-painted ears (Figure 5H-J), although effects were smaller in magnitude than in MRL/lpr and B6.Sle1yaa models. Unlike the IMQ-treated wildtype mice, however, IMQ-treated LC-AD17 mice did not show reduction in ear swelling or epidermal permeability with anti-IFNAR1 (Figure 5I-J). These results suggested that the ameliorative effects of anti-IFNAR1 on photosensitivity in the IMQ model was dependent on LC ADAM17. Together, the dependence of anti-IFNAR1-driven reduction in photosensitivity on EGFR and LC ADAM17 across multiple lupus models provides strong support for the idea that IFN-I contributes to photosensitivity by causing LC ADAM17 dysfunction. These results also suggest that the beneficial effects on SLE skin of anifrolumab (anti-IFNAR1) may be due at least in part to improving LC ADAM17 activity.

DISCUSSION

Here, we establish that IFN-I can cause LC ADAM17 dysfunction and that this IFN-I-mediated LC ADAM17 dysfunction is a mechanism by which IFN-I contributes to photosensitivity in lupus models. Our results provide insight into the pathogenic contributions of IFN-I to cutaneous disease in lupus and suggest that the beneficial effects of anifrolumab on skin disease in human SLE may be in part attributable to the restoration of LC ADAM17 activity. Our results further point to LC dysfunction as a central player and potential therapeutic target in lupus photosensitivity.

IFN-I has been shown to directly prime keratinocytes for UVR-induced apoptosis (Sarkar et al., 2018) and our results establishing that LC ADAM17 dysfunction is an important mechanism do not rule out the importance of a keratinocyte-intrinsic mechanism. IFN-I could both indirectly contribute to increasing UVR-induced keratinocyte apoptosis via LC dysfunction and directly prime keratinocytes for death. More work to fully understand the ways in which IFN-I contributes to photosensitivity will help to refine therapeutic approaches.

Our results both point to the utility of targeting the increased IFN-I in lupus models and underscore the need to preserve homeostatic IFN-I functions. That the higher 500 µg/dose of anti-IFNAR1, despite correcting LC ADAM17 function, did not reduce epidermal permeability or inflammatory cell infiltration suggests that, even in the diseased state, IFN-I has protective skin-intrinsic functions that are important to maintain. Clinically, patients with high IFN-I scores responded to anifrolumab (Morand et al., 2020) and, when comparable, with a greater effect size than patients with lower IFN-I scores (Furie et al., 2017). Thus, trial data are consistent with the idea that excessive IFN-I in SLE is pathogenic, with our findings suggesting that one of the pathogenic roles is in causing LC ADAM17 dysfunction. Better understanding whether the

contexts in which IFN-I is protective or pathogenic is a function of purely quantitative differences or of distinct cellular sources and sensors will help to refine IFN-I-targeting therapies.

Further studies are needed to understand how exactly IFNAR regulates LC ADAM17 activity and the additional contributions of LC ADAM17 to tissue function. IFNα has been shown to induce ADAM17 expression and activity in bone marrow-derived dendritic cell cultures (Anthony et al., 2015) while IFNγ has been shown to downregulate ADAM17 expression in hepatic stellate cells (Fujita et al., 2006), and whether LC-intrinsic IFNAR on LCs signal to modulate LC ADAM17 is among the questions that remain to be addressed. Moreover, ADAM17 has multiple substrates (Zunke and Rose-John, 2017), suggesting additional mechanisms by which LC ADAM17 dysfunction contributes to CLE and SLE.

The shared upregulation of the IFN-I pathway in human lupus non-lesional skin and multiple lupus mouse models reinforces the idea that a high IFN-I environment in skin contributes to disease pathogenesis. Keratinocytes are a potential source of local IFN-I (Sarkar et al., 2018), and the recent success in targeting BDCA2 in lupus (Furie et al., 2019) suggests that IFN-I-producing plasmacytoid dendritic cells, whether circulating or local to skin, also contributes. The increasing evidence pointing to an IFN signature in non-lesional skin in human SLE (Der et al., 2019), CLE (Figure 1), incomplete SLE (Lambers et al., 2019), and now multiple lupus mouse models (Figure 1) as well as the importance of IFN-I to lupus skin disease (Furie et al., 2017; Morand et al., 2020; Nickerson et al., 2013) (Figure 4), helps to better understand how to use IFN-I signatures in non-lesional skin in diagnosis or patient stratification assessment.

Our results underscore a key role for LCs in disease pathogenesis in lupus models. Previously, we showed that LC ADAM17 dysfunction contributed to photosensitivity in both wildtype mice and SLE models (Shipman et al., 2018). Here, our results suggesting that correcting LC dysfunction can reduce photosensitivity and pointing to the central role of LCs in anti-IFNAR1-mediated effects further indicate that LCs should be considered as a therapeutic target for cutaneous disease in lupus. While anifrolumab and JAK inhibitors, such as tofacitinib, could be used to correct LC dysfunction, specific targeting of LC function may be useful for preserving protective IFN-I functions.

METHODS

Mice

8-16 week old mice were used unless otherwise specified. Mice were sex- and age-matched. For C57Bl/6 mice, LCAd17 (Langerin-cre;Adam17 f/f) mice, and wildtype littermate controls, males and females were used. Unless otherwise indicated, for MRL/+ and MRL/lpr mice, females were used at 8-12 weeks, while males were used at 12-16 weeks as females present with a disease phenotype earlier than males do. For B6.Sle1yaa mice and their B6 controls, only males were used because the model depends on the autoimmune accelerator locus located on the Y chromosome. B6 mice were either bred in-house or purchased from Jackson Laboratory (Bar Harbor, ME). MRL/+, MRL/lpr mice, B6.Sle1yaa mice and their B6 controls were either purchased from Jackson Laboratory or bred in-house from purchased breeders. LCAd17 mice (Shipman et al., 2018) were bred in-house. All animal procedures were performed in accordance with the regulations of the Institutional Animal Care and Use Committee at Weill Cornell Medicine (New York, NY)

Mouse treatments

For IFN-κ painting, 37.5 ng IFN-κ (R&D Systems, Minneapolis, MN) was dissolved in DMSO (Sigma Aldrich, St. Louis, MO) and was applied topically onto each ear (18.75 ng on dorsal and ventral sides, each). For anti-IFNAR11 treatments, mice were injected i.p. with 500 µg/dose or 125 µg/dose of anti-IFNAR11 (MAR1-5A3) or isotype control (MOPC-21) (Bio X Cell, West Lebanon, NH). For UVR treatments, mice were exposed to 250 J/m^2 for four consecutive days using a bank of four FS40T12 sunlamps, as previously described (Shipman et al., 2018). To measure ear swelling after UVR exposure, a caliper (Mitutoyo, Aurora, IL) was used to take

three measurements throughout each ear, and the reported value is the average of both ears. Each measurement was taken 22-24 hours after the previous measurement. For the imiquimod (IMQ)-induced lupus mouse model, mice were painted on the dorsal and ventral sides of both ears with 5% imiquimod cream (42 mg/ear/mouse) 3x/week for 5-6 weeks (Yokogawa et al., 2014) prior to and continued through experiments. Indicated mice received 2.95 mg of the irreversible EGFR inhibitor PD168393 (0.74 mg on dorsal and ventral sides, each) (Selleck Chem, Pittsburgh, PA).

Human subjects

For microarray analysis, seven CLE patients with the discoid subtype of CLE were examined. Both lesional and non-lesional skin were collected and the gene expression data from lesional tissue of these patients have been published, and patient characteristics are described (Jabbari et al., 2014). Healthy controls include the three that were previously described. All human tissue collection and research use adhered to protocols approved by the Institutional Review and Privacy Boards at the Rockefeller University (IRB# AJA-00740) and New York University (IRB# 10-02117), where participants signed written informed consents.

For suction blistering, 3 female and 1 male healthy participants between the ages of 23 and 55 participated. All human tissue collection and research use adhered to protocols approved by the Institutional Review and Privacy Board at the Hospital for Special Surgery (IRB# 2019-1998), where participants signed written informed consents.

Human skin cell collection and preparation

Suction blistering was performed as previously described (27). Eight 5 mm suction blisters were generated with a negative pressure instrument (NP-4 model, Electronic Diversities, Finksburg, MD) on the arm of healthy donors over 30-60 minutes. The blister fluid was then collected by aspiration, and epidermal roofs were collected. After collection, epidermal roofs from suction blisters were digested with dispase (2.42 U/mL; Thermo Fisher Scientific, Waltham, MA), collagenase type II (616 U/mL; Worthington Biochemical Corporation, Lakewood, NJ), and DNAseI (80 μg/mL; Sigma Aldrich, St. Louis, MO) for 40 minutes to generate single cell suspensions that were used for the ADAM17 sheddase assay.

Skin cell collection and low cytometry staining and quantification

For murine epidermal single cell suspensions, skin on the trunk was excised and subcutaneous fat scraped off. Skin was incubated in dispase (2.42 U/mL) at 37°C. The epidermis was then gently peeled, finely minced, digested in type II collagenase (616 U/mL) and DNAseI (80 μg/mL).

For collection of ear skin, ears were cut along the cartilage ridge, and the dorsal and ventral sides were manually peeled. Ear skin was then finely minced and digested with a buffer containing dispase, type II collagenase, and DNAseI as described above. For murine Langerhans cell TNFR1 staining for the ADAM17 sheddase activity assay (see below), epidermal cells were preincubated with Fc block and then stained so that we could gate on CD45+, CD3-, CD11c+, I-Ab+ for B6 mice and I-Ak+ for MRL mice, EpCAM+ LCs and assess for TNFR1. Langerhans cells were sometimes stained with rabbit-anti-ADAM17 (Lora et al., 2021) followed by donkey anti-rabbit IgG (Jackson Immunoresearch, West Grove, PA). Monocytes and T cells were

identified by gating for CD45+CD11b+Ly6C+ and CD45+CD11c-I-Ak/I-Ab-CD3+ cells, respectively. 4',6-diamidino-2-phenylindole dihydrochloride (DAPI) was used to exclude dead cells and debris (Sigma Aldrich, St. Louis, MO). All antibodies are from Biolegend, San Diego, CA unless otherwise indicated.

For human Langerhans cell TNFR1 staining for the ADAM17 sheddase activity assay, single cell suspensions of the epidermal roofs of suction blisters and blister fluid were preincubated with Fc block and subsequently stained for CD45+, CD11c+, CD14-, CD3- CD19-, CD56-, CD66b-, EpCAM+, and HLA-DR+ to identify LCs. DAPI was used to exclude dead cells and debris, and TNFR1 were also stained to assess ADAM17 activity. All antibodies are from Biolegend, San Diego, CA unless otherwise indicated. Cells were analyzed using a FACSCanto or FACSymphony A3 (BD Biosciences, San Jose, CA) and data were analyzed with FlowJo V10 Software (TreeStar, Ashland, OR).

For mean fluorescent intensity (MFI) calculations of TNFR1, each sample was assayed in triplicate, and the mean of the triplicates was recorded unless otherwise specified. The MFI of TNFR1 was divided by the MFI for the isotype control to generate a relative MFI. The percent TNFR1 MFI change was calculated by setting the relative MFI of the control sample to 1, and normalizing the value from the experimental samples to that control. In experiments where there was more than one control sample, the control values were averaged, and the experimental samples were each normalized to the averaged value.

Ex vivo ADAM17 sheddase activity assay

For murine skin, single cell suspensions of epidermis were incubated for 16-20 hours with IFN-κ (3.125 ng/mL) (R&D Systems, Minneapolis, MN) at 500,000 cells/mL of RPMI (Corning,

Edison, New Jersey) with HEPES buffer, L-glutamine, penicillin-streptomycin and 10% fetal calf serum (all Thermo Fisher Scientific, Waltham, MA). Cells were then exposed to 500 J/m^2 UVR, as previous (Shipman et al., 2018)and incubated for an additional 45 minutes and prior to staining for cell surface markers described above. Indicated samples were treated with tofacitinib (Selleck Chem, Pittsburgh, PA) at 1 nM during IFN-κ incubation.

For human skin, cells were incubated for 1 hour with recombinant human IFN-β (35.7 ng/mL; activity=2.8x10^8 UI/mg) and then exposed to 500 J/m^2 UVR as above. Cells were further incubated for 45 minutes and collected for preincubation with Fc block. Cells were then stained for cell surface markers described above.

Epidermal permeability assay

Epidermal barrier function was assessed as described (Shipman et al., 2018). Ear skin was dehydrated and rehydrated in graded methanol and then incubated in 0.1% toluidine blue dye (Sigma Aldrich, St. Louis, MO). The dye was extracted with a buffer consisting of 95% methanol, 2.5% sulfuric acid, and 2.5% water and quantified with a colorimeter at 620 nm. Dye concentration was calculated using a standard curve.

RNA-Sequencing

Female MRL/+ and MRL/lpr 12-14 weeks old and 12 week old B6 and B6.Sle1yaa male mice were used for RNA sequencing. RNA was extracted from ear skin using an RNEasy Kit (Qiagen, Germantown, MD) and quality confirmed on a BioAnalyzer 2100 (Agilent Technologies, Santa Clara, CA). Libraries were prepared with non-stranded and poly-A selection TruSeq RNA Sample Preparation kits. Sequencing libraries were sequenced by the Genomics Core Facility at

Weill Cornell Medicine using a HiSeq 2500 (MRL/lpr, MRL/+ samples) and NovaSeq (B6, B6.Sle1yaa) at a depth of 15-30 million mappable paired-end reads per sample.

Computational analyses of gene expression data

Microarray analysis was performed using healthy controls from an existing GEO dataset (GSE52471) obtained from GEO using GEOquery and combined with non-lesional skin sample data kindly provide provided by the authors of the original study (Jabbari et al., 2014). Microarrays data were normalized with gcRMA normalization using the gcrma R package (Wu et al., 2021). Differential gene expression analysis was performed with limma using the empirical bayes method (Ritchie et al., 2015) and controlling for microarray hybridization kit and sex, Batch correction was performed using ComBat (Leek et al., 2021). Visualizations were generated using ComBat corrected data with plotly and ggplot2 in R.

For RNA sequencing analysis, read quality filtering and adapter trimming were performed using *fastp* (Chen et al., 2018). Filtered reads were mapped to the mouse genome (mm10), and exonic reads were counted against GENCODE release 27 annotation with the STAR aligner (Dobin et al., 2013) using a customised pipeline available at https://gitlab.com/hssgenomics/pipelines. Differential gene expression analysis was performed with edgeR 3.30.2 using quasi-likelihood framework. Genes with low expression levels (<3 counts per million in at least one group) were filtered from all downstream analyses. P values were adjusted to correct for multiple testing using the Benhamini-Hochberg FDR procedure. Genes with adjusted P values < 0.01 were considered differentially expressed. Downstream analyses were performed in R using a Shiny-driven visualization platform (RNAseq DRaMA) developed at the HSS David Z. Rosensweig Genomics Research Center.

Differentially regulated pathways we identified using R QuSAGE 2.22.0 package (Yaari et al., 2013) with MSigDB C2 set (curated gene sets). All gene set with less than 10 genes were not included in the analysis. Pathways with Benhamini-Hochberg adjusted pvalues <0.005 (non-lesional skin versus healthy control) or <0.05(MRL/lpr versus MRL/+) were used for further analyses.

Ranked GSEA analysis was performed to define gene sets from MSigDB C2 enriched in human non-lessional skin and MRL/lpr mouse. Log transformed fold changes in relevant comparisons (non-lesional skin versus healthy control and MRL/lpr versus MRL/+) were used as a ranking variables. Pathways with Benhamini-Hochberg adjusted pvalues <0.05 were selected and the pathways similarity network was build to visualize gene overlap between pathways using R package *hypeR* (1.7.0) (Federico and Monti, 2020) and compare enriched pathways in human SLE patients and mouse models.

Statistics

Unpaired and paired Student's t-test were used to evaluate p-values as indicated. Significance was defined as $p<0.05$.

AUTHOR CONTRIBUTIONS

TML, KRV, and NS designed and performed experiments and interpreted data. YC and DJO analyzed and interpreted data. AJ and JGK provided data. JL and CPB provided reagents and insightful discussion. YL, MJS, IFS, WGA, and NA contributed to experiments. WDS and MR designed experimental protocols. TML and TTL were responsible for the conceptual planning of the project. TTL supervised experiments and interpreted data. TML, YC, and TTL wrote the manuscript, and all authors critically read the manuscript and provided feedback.

ACKNOWLEDGEMENTS

This work was supported by Alpha Omega Alpha Carolyn L. Kuckein Student Research Fellowship (TML), NIAMS K08 AR069111 to the University of Iowa Department of Dermatology (AJ), VA Merit I01 BX004907 (AJ), Physician Scientist Career Development Award from the Dermatology Foundation (AJ), NIH MSTP T32GM007739 to the Weill Cornell/Rockefeller/Sloan-Kettering Tri-Institutional MD-PhD Program (WDS), NIH T32AR071302-01 to the Hospital for Special Surgery Research Institute Rheumatology Training Program (WDS), the National Institutes of Health R35GM134907 (CPB) and R01AI079178 (TTL), the Lupus Research Alliance (TTL), the St. Giles Foundation (TTL), and by the NIH Office of the Director grant S10OD019986 to Hospital for Special Surgery.

LIST OF FIGURES, SUPPLEMENTAL FIGURES, AND TABLES:

Figure 1. Non-lesional skin in human CLE and multiple murine lupus models share upregulated interferon (IFN) signature.

Figure 2. IFN-I can reduce LC ADAM17 sheddase activity.

Figure 3. Anti-IFNAR1 restores LC ADAM17 activity in multiple lupus models.

Figure 4. Anti-IFNAR1 reduces photosensitivity in MRL/lpr mice.

Figure 5. Reduction of photosensitivity by anti-IFNAR1 is dependent on EGFR and LC ADAM17.

Figure S1. Further analyses of gene expression in human CLE and multiple murine lupus models.

Figure S2. ADAM17 expression levels in LCAd17 mice, UVR-induced cell surface TNFR1 loss on LCs in mixed epidermal cell suspensions is dependent on LC ADAM17, and LCAd17 mice show UVR-induced ear swelling.

Figure S3. Langerhans cell yield and gating with suction blistering of human skin.

Table S1. Differentially expressed genes in CLE vs healthy control non-lesional skin microarray

Table S2. Differential expressed pathways in CLE vs healthy control non-lesional skin using QuSAGE

Table S3. Differentially expressed genes in MRL/lpr vs control MRL/+ non-lesional skin RNAseq

Table S4. Differential expressed pathways in MRL/lpr vs control MRL/+ non-lesional skin using QuSAGE

Table S5. Ranked GSEA enriched pathways in CLE vs healthy control dataset.

Table S6. Differentially expressed genes in B6.Sle1yaa vs control B6 non-lesional skin RNAseq

REFERENCES

Anthony, S.M., M.E. Howard, Y. Hailemichael, W.W. Overwijk, and K.S. Schluns. 2015. Soluble interleukin-15 complexes are generated in vivo by type I interferon dependent and independent pathways. *PLoS ONE* 10:e0120274-e0120274.

Baechler, E.C., F.M. Batliwalla, G. Karypis, P.M. Gaffney, W.A. Ortmann, K.J. Espe, K.B. Shark, W.J. Grande, K.M. Hughes, V. Kapur, P.K. Gregersen, and T.W. Behrens. 2003. Interferon-inducible gene expression signature in peripheral blood cells of patients with severe lupus. *PNAS* 100:2610-2615.

Bennett, L., A.K. Palucka, E. Arce, V. Cantrell, J. Borvak, J. Banchereau, and V. Pascual. 2003. Interferon and Granulopoiesis Signatures in Systemic Lupus Erythematosus Blood. *J. Exp. Med.* 197:711-723.

Boukhaled, G.M., S. Harding, and D.G. Brooks. 2021. Opposing Roles of Type I Interferons in Cancer Immunity. *Annual Review of Pathology: Mechanisms of Disease* 16:167-198.

Chen, S., Y. Zhou, Y. Chen, and J. Gu. 2018. fastp: an ultra-fast all-in-one FASTQ preprocessor. *Bioinformatics* 34:i884-i890.

Crow, M.K. 2014. Type I interferon in the pathogenesis of lupus. *J Immunol* 192:5459-5468.

Crow, M.K., and L. Ronnblom. 2019. Type I interferons in host defence and inflammatory diseases. *Lupus Sci Med* 6:e000336.

Der, E., S. Ranabothu, H. Suryawanshi, K.M. Akat, R. Clancy, P. Morozov, M. Kustagi, M. Czuppa, P. Izmirly, H.M. Belmont, T. Wang, N. Jordan, N. Bornkamp, J. Nwaukoni, J. Martinez, B. Goilav, J.P. Buyon, T. Tuschl, and C. Putterman. 2017. Single cell RNA sequencing to dissect the molecular heterogeneity in lupus nephritis. *JCI Insight* 2:

Der, E., H. Suryawanshi, P. Morozov, M. Kustagi, B. Goilav, S. Ranabothu, P. Izmirly, R. Clancy, H.M. Belmont, M. Koenigsberg, M. Mokrzycki, H. Rominieki, J.A. Graham, J.P. Rocca, N. Bornkamp, N. Jordan, E. Schulte, M. Wu, J. Pullman, K. Slowikowski, S. Raychaudhuri, J. Guthridge, J. James, J. Buyon, T. Tuschl, and C. Putterman. 2019. Tubular cell and keratinocyte single-cell transcriptomics applied to lupus nephritis reveal type I IFN and fibrosis relevant pathways. *Nat Immunol* 20:915-927.

Dobin, A., C.A. Davis, F. Schlesinger, J. Drenkow, C. Zaleski, S. Jha, P. Batut, M. Chaisson, and T.R. Gingeras. 2013. STAR: ultrafast universal RNA-seq aligner. *Bioinformatics* 29:15-21.

Federico, A., and S. Monti. 2020. hypeR: an R package for geneset enrichment workflows. *Bioinformatics* 36:1307-1308.

Fujita, T., C. Maesawa, K. Oikawa, H. Nitta, G. Wakabayashi, and T. Masuda. 2006. Interferon-gamma down-regulates expression of tumor necrosis factor-alpha converting enzyme/a disintegrin and metalloproteinase 17 in activated hepatic stellate cells of rats. *Int J Mol Med* 17:605-616.

Furie, R., M. Khamashta, J.T. Merrill, V.P. Werth, K. Kalunian, P. Brohawn, G.G. Illei, J. Drappa, L. Wang, and S. Yoo. 2017. Anifrolumab, an Anti-Interferon-α Receptor Monoclonal Antibody, in Moderate-to-Severe Systemic Lupus Erythematosus. *Arthritis Rheumatol* 69:376-386.

Furie, R., V.P. Werth, J.F. Merola, L. Stevenson, T.L. Reynolds, H. Naik, W. Wang, R. Christmann, A. Gardet, A. Pellerin, S. Hamann, P. Auluck, C. Barbey, P. Gulati, D. Rabah, and N. Franchimont. 2019. Monoclonal antibody targeting BDCA2 ameliorates skin lesions in systemic lupus erythematosus. *J Clin Invest* 129:1359-1371.

Goel, R.R., X. Wang, L.J. O'Neil, S. Nakabo, K. Hasneen, S. Gupta, G. Wigerblad, L.P. Blanco, J.B. Kopp, M.I. Morasso, S.V. Kotenko, Z.X. Yu, C. Carmona-Rivera, and M.J. Kaplan. 2020. Interferon lambda promotes immune dysregulation and tissue inflammation in TLR7-induced lupus. *Proc Natl Acad Sci U S A* 117:5409-5419.

Gregorio, J., S. Meller, C. Conrad, A. Di Nardo, B. Homey, A. Lauerma, N. Arai, R.L. Gallo, J. Digiovanni, and M. Gilliet. 2010. Plasmacytoid dendritic cells sense skin injury and promote wound healing through type I interferons. *J Exp Med* 207:2921-2930.

Jabbari, A., M. Suárez-Fariñas, J. Fuentes-Duculan, J. Gonzalez, I. Cueto, A.G. Franks, Jr., and J.G. Krueger. 2014. Dominant Th1 and minimal Th17 skewing in discoid lupus revealed by transcriptomic comparison with psoriasis. *J Invest Dermatol* 134:87-95.

Jenks, S.A., K.S. Cashman, E. Zumaquero, U.M. Marigorta, A.V. Patel, X. Wang, D. Tomar, M.C. Woodruff, Z. Simon, R. Bugrovsky, E.L. Blalock, C.D. Scharer, C.M. Tipton, C. Wei, S.S. Lim, M. Petri, T.B. Niewold, J.H. Anolik, G. Gibson, F.E.-H. Lee, J.M. Boss, F.E. Lund, and I. Sanz. 2018. Distinct Effector B Cells Induced by Unregulated Toll-like Receptor 7 Contribute to Pathogenic Responses in Systemic Lupus Erythematosus. *Immunity* 49:725-739.e726.

Kahlenberg, J.M. 2021. Rethinking the Pathogenesis of Cutaneous Lupus. *J Invest Dermatol* 141:32-35.

Kirou, K.A., C. Lee, S. George, K. Louca, I.G. Papagiannis, M.G. Peterson, N. Ly, R.N. Woodward, K.E. Fry, A.Y. Lau, J.G. Prentice, J.G. Wohlgemuth, and M.K. Crow. 2004. Coordinate overexpression of interferon-alpha-induced genes in systemic lupus erythematosus. *Arthritis Rheum* 50:3958-3967.

Lambers, W.M., K. de Leeuw, B. Doornbos-van der Meer, G.F.H. Diercks, H. Bootsma, and J. Westra. 2019. Interferon score is increased in incomplete systemic lupus erythematosus and correlates with myxovirus-resistance protein A in blood and skin. *Arthritis Research & Therapy* 21:260.

Leek, J.T., W.E. Johson, H.S. Parker, E.J. Fertig, A.E. Jaffe, Y. Zhang, J.D. Storey, and L. Callado Torres. 2021. sva: Surrogate Variable Analysis. . *R package version 3.40.0*

Lessard, J.C., S. Piña-Paz, J.D. Rotty, R.P. Hickerson, R.L. Kaspar, A. Balmain, and P.A. Coulombe. 2013. Keratin 16 regulates innate immunity in response to epidermal barrier breach. *Proc Natl Acad Sci U S A* 110:19537-19542.

Lora, J., G. Weskamp, T.M. Li, T. Maretzky, D.T.N. Shola, S. Monette, S.F. Lichtenthaler, T.T. Lu, C. Yang, and C.P. Blobel. 2021. Targeted truncation of the ADAM17 cytoplasmic domain in mice results in protein destabilization and a hypomorphic phenotype. *J Biol Chem* 296:100733.

Morand, E.F., R. Furie, Y. Tanaka, I.N. Bruce, A.D. Askanase, C. Richez, S.C. Bae, P.Z. Brohawn, L. Pineda, A. Berglind, and R. Tummala. 2020. Trial of Anifrolumab in Active Systemic Lupus Erythematosus. *N Engl J Med* 382:211-221.

Nickerson, K.M., J.L. Cullen, M. Kashgarian, and M.J. Shlomchik. 2013. Exacerbated Autoimmunity in the Absence of TLR9 in MRL.Fas^{lpr} Mice Depends on Ifnar1. *The Journal of Immunology* 190:3889-3894.

Patel, J., R. Borucki, and V.P. Werth. 2020. An Update on the Pathogenesis of Cutaneous Lupus Erythematosus and Its Role in Clinical Practice. *Curr Rheumatol Rep* 22:69.

Pisitkun, P., J.A. Deane, M.J. Difilippantonio, T. Tarasenko, A.B. Satterthwaite, and S. Bolland. 2006. Autoreactive B cell responses to RNA-related antigens due to TLR7 gene duplication. *Science* 312:1669-1672.

Ritchie, M.E., B. Phipson, D. Wu, Y. Hu, C.W. Law, W. Shi, and G.K. Smyth. 2015. limma powers differential expression analyses for RNA-sequencing and microarray studies. *Nucleic Acids Res* 43:e47.

Rodero, M.P., and Y.J. Crow. 2016. Type I interferon–mediated monogenic autoinflammation: The type I interferonopathies, a conceptual overview. *Journal of Experimental Medicine* 213:2527-2538.

Roy, E.R., B. Wang, Y.-w. Wan, G. Chiu, A. Cole, Z. Yin, N.E. Propson, Y. Xu, J.L. Jankowsky, Z. Liu, V.M.Y. Lee, J.Q. Trojanowski, S.D. Ginsberg, O. Butovsky, H. Zheng, and W. Cao. 2020. Type I interferon response drives neuroinflammation and synapse loss in Alzheimer disease. *The Journal of Clinical Investigation* 130:1912-1930.

Sarkar, M.K., G.A. Hile, L.C. Tsoi, X. Xing, J. Liu, Y. Liang, C.C. Berthier, W.R. Swindell, M.T. Patrick, S. Shao, P.-S. Tsou, R. Uppala, M.A. Beamer, A. Srivastava, S.L. Bielas, P.W. Harms, S. Getsios, J.T. Elder, J.J. Voorhees, J.E. Gudjonsson, and J.M. Kahlenberg. 2018. Photosensitivity and type I IFN responses in cutaneous lupus are driven by epidermal-derived interferon kappa. *Annals of the Rheumatic Diseases* 77:1653-1664.

Shipman, W.D., S. Chyou, A. Ramanathan, P.M. Izmirly, S. Sharma, T. Pannellini, D.C. Dasoveanu, X. Qing, C.M. Magro, R.D. Granstein, M.A. Lowes, E.G. Pamer, D.H. Kaplan, J.E. Salmon, B.J. Mehrara, J.W. Young, R.M. Clancy, C.P. Blobel, and T.T. Lu. 2018. A protective Langerhans cell–keratinocyte axis that is dysfunctional in photosensitivity. *Science Translational Medicine* 10:

Sim, J.H., W.G. Ambler, I.F. Sollohub, M.J. Howlader, T.M. Li, H.J. Lee, and T.T. Lu. 2021. Immune Cell–Stromal Circuitry in Lupus Photosensitivity. *The Journal of Immunology* 206:302-309.

Snell, L.M., T.L. McGaha, and D.G. Brooks. 2017. Type I Interferon in Chronic Virus Infection and Cancer. *Trends in Immunology* 38:542-557.

Sontheimer, C., D. Liggitt, and K.B. Elkon. 2017. Ultraviolet B Irradiation Causes Stimulator of Interferon Genes–Dependent Production of Protective Type I Interferon in Mouse Skin by Recruited Inflammatory Monocytes. *Arthritis & Rheumatology* 69:826-836.

Strassner, J.P., M. Rashighi, M. Ahmed Refat, J.M. Richmond, and J.E. Harris. 2017. Suction blistering the lesional skin of vitiligo patients reveals useful biomarkers of disease activity. *J Am Acad Dermatol* 76:847-855.e845.

Subramanian, S., K. Tus, Q.Z. Li, A. Wang, X.H. Tian, J. Zhou, C. Liang, G. Bartov, L.D. McDaniel, X.J. Zhou, R.A. Schultz, and E.K. Wakeland. 2006. A Tlr7 translocation accelerates systemic autoimmunity in murine lupus. *Proc Natl Acad Sci U S A* 103:9970-9975.

Tsoi, L.C., G.A. Hile, C.C. Berthier, M.K. Sarkar, T.J. Reed, J. Liu, R. Uppala, M. Patrick, K. Raja, X. Xing, E. Xing, K. He, J.E. Gudjonsson, and J.M. Kahlenberg. 2019. Hypersensitive IFN Responses in Lupus Keratinocytes Reveal Key Mechanistic Determinants in Cutaneous Lupus. *The Journal of Immunology* 202:2121-2130.

Wu, J., R. Irizarry, J. MadDonald, and J. Gentry. 2021. gcrma: Background Adjustment Using Sequence Information. . *R package version 2.64.0*

Yaari, G., C.R. Bolen, J. Thakar, and S.H. Kleinstein. 2013. Quantitative set analysis for gene expression: a method to quantify gene set differential expression including gene-gene correlations. *Nucleic Acids Res* 41:e170.

Yokogawa, M., M. Takaishi, K. Nakajima, R. Kamijima, C. Fujimoto, S. Kataoka, Y. Terada, and S. Sano. 2014. Epicutaneous application of toll-like receptor 7 agonists leads to

systemic autoimmunity in wild-type mice: a new model of systemic Lupus erythematosus. *Arthritis Rheumatol* 66:694-706.

Zunke, F., and S. Rose-John. 2017. The shedding protease ADAM17: Physiology and pathophysiology. *Biochimica et Biophysica Acta (BBA) - Molecular Cell Research* 1864:2059-2070.

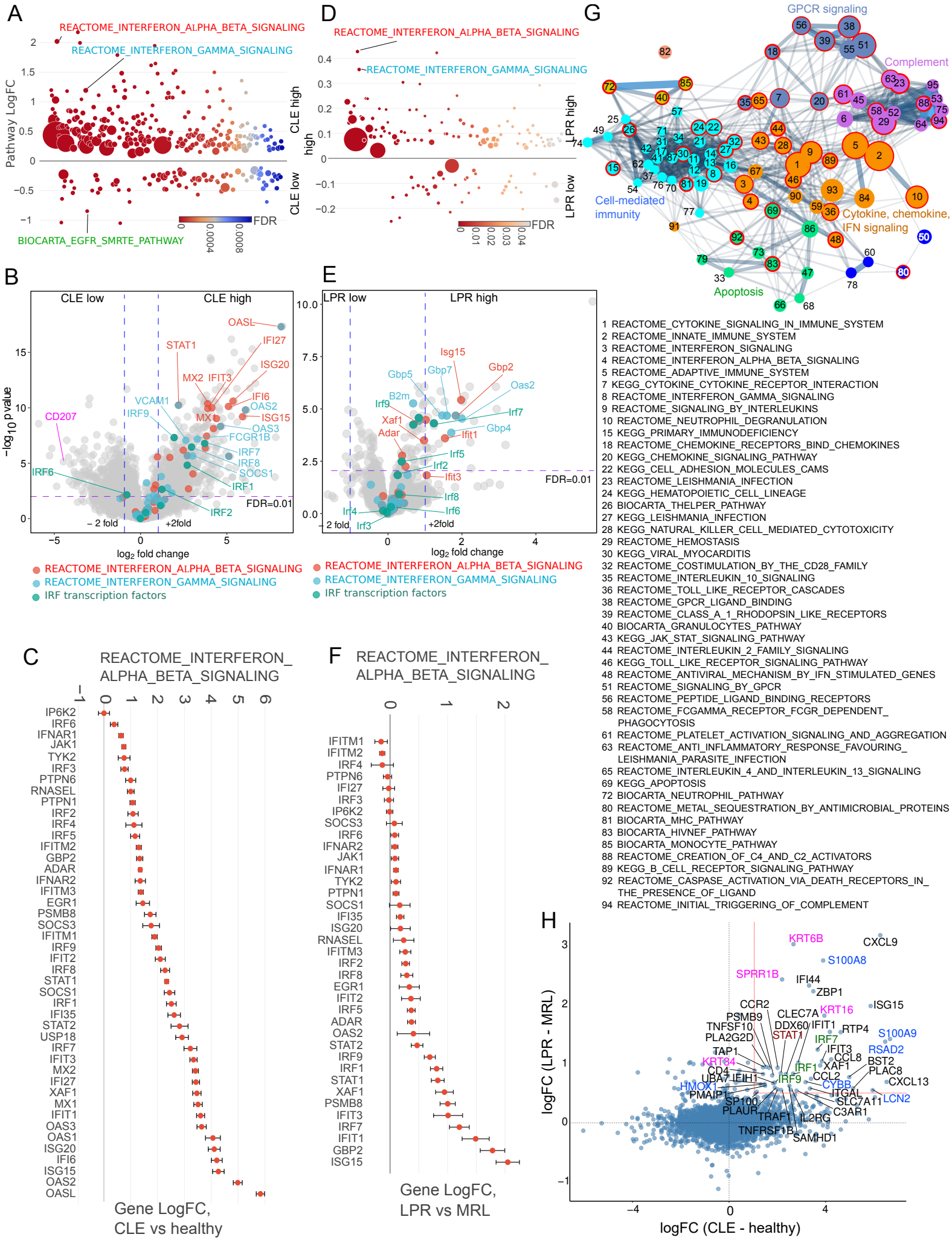
A
REACTOME_INTERFERON_ALPHA_BETA_SIGNALING
REACTOME_INTERFERON_GAMMA_SIGNALING
Pathway LogFC
BIOCARTA_EGFR_SMRTE_PATHWAY
FDR
D
CLE high
CLE low
LPR high
LPR low
G
GPCR signaling
Complement
Cell-mediated immunity
Cytokine, chemokine, IFN signaling
Apoptosis
B
CLE low
CLE high
−log10 p value
log2 fold change
FDR=0.01
− 2 fold
+2fold
REACTOME_INTERFERON_ALPHA_BETA_SIGNALING
REACTOME_INTERFERON_GAMMA_SIGNALING
IRF transcription factors
E
LPR low
LPR high
FDR=0.01
2 fold
+2fold
REACTOME_INTERFERON_ALPHA_BETA_SIGNALING
REACTOME_INTERFERON_GAMMA_SIGNALING
IRF transcription factors
1 REACTOME_CYTOKINE_SIGNALING_IN_IMMUNE_SYSTEM
2 REACTOME_INNATE_IMMUNE_SYSTEM
3 REACTOME_INTERFERON_SIGNALING
4 REACTOME_INTERFERON_ALPHA_BETA_SIGNALING
5 REACTOME_ADAPTIVE_IMMUNE_SYSTEM
7 KEGG_CYTOKINE_CYTOKINE_RECEPTOR_INTERACTION
8 REACTOME_INTERFERON_GAMMA_SIGNALING
9 REACTOME_SIGNALING_BY_INTERLEUKINS
10 REACTOME_NEUTROPHIL_DEGRANULATION
15 KEGG_PRIMARY_IMMUNODEFICIENCY
18 REACTOME_CHEMOKINE_RECEPTORS_BIND_CHEMOKINES
20 KEGG_CHEMOKINE_SIGNALING_PATHWAY
22 KEGG_CELL_ADHESION_MOLECULES_CAMS
23 REACTOME_LEISHMANIA_INFECTION
24 KEGG_HEMATOPOIETIC_CELL_LINEAGE
26 BIOCARTA_THELPER_PATHWAY
27 KEGG_LEISHMANIA_INFECTION
28 KEGG_NATURAL_KILLER_CELL_MEDIATED_CYTOTOXICITY
29 REACTOME_HEMOSTASIS
30 KEGG_VIRAL_MYOCARDITIS
32 REACTOME_COSTIMULATION_BY_THE_CD28_FAMILY
35 REACTOME_INTERLEUKIN_10_SIGNALING
36 REACTOME_TOLL_LIKE_RECEPTOR_CASCADES
38 REACTOME_GPCR_LIGAND_BINDING
39 REACTOME_CLASS_A_1_RHODOPSIN_LIKE_RECEPTORS
40 BIOCARTA_GRANULOCYTES_PATHWAY
43 KEGG_JAK_STAT_SIGNALING_PATHWAY
44 REACTOME_INTERLEUKIN_2_FAMILY_SIGNALING
46 KEGG_TOLL_LIKE_RECEPTOR_SIGNALING_PATHWAY
48 REACTOME_ANTIVIRAL_MECHANISM_BY_IFN_STIMULATED_GENES
51 REACTOME_SIGNALING_BY_GPCR
56 REACTOME_PEPTIDE_LIGAND_BINDING_RECEPTORS
58 REACTOME_FCGAMMA_RECEPTOR_FCGR_DEPENDENT_PHAGOCYTOSIS
61 REACTOME_PLATELET_ACTIVATION_SIGNALING_AND_AGGREGATION
63 REACTOME_ANTI_INFLAMMATORY_RESPONSE_FAVOURING_LEISHMANIA_PARASITE_INFECTION
65 REACTOME_INTERLEUKIN_4_AND_INTERLEUKIN_13_SIGNALING
69 KEGG_APOPTOSIS
72 BIOCARTA_NEUTROPHIL_PATHWAY
80 REACTOME_METAL_SEQUESTRATION_BY_ANTIMICROBIAL_PROTEINS
81 BIOCARTA_MHC_PATHWAY
83 BIOCARTA_HIVNEF_PATHWAY
85 BIOCARTA_MONOCYTE_PATHWAY
88 REACTOME_CREATION_OF_C4_AND_C2_ACTIVATORS
89 KEGG_B_CELL_RECEPTOR_SIGNALING_PATHWAY
92 REACTOME_CASPASE_ACTIVATION_VIA_DEATH_RECEPTORS_IN_THE_PRESENCE_OF_LIGAND
94 REACTOME_INITIAL_TRIGGERING_OF_COMPLEMENT
C
REACTOME_INTERFERON_ALPHA_BETA_SIGNALING
Gene LogFC, CLE vs healthy
F
REACTOME_INTERFERON_ALPHA_BETA_SIGNALING
Gene LogFC, LPR vs MRL
H
logFC (LPR - MRL)
logFC (CLE - healthy)

Figure 1

Figure 1. Non-lesional skin in human CLE and multiple murine lupus models share upregulated interferon (IFN) signature. Non-lesional skin gene expression from (A-C) human CLE patients (N=7) and healthy controls (N=13) analyzed by microarray and (D-F) MRL/lpr (LPR) (N=8) and control MRL/+ (MRL) (N=9) mice analyzed by RNA sequencing. (A, D) Differentially expressed pathways were determined using QuSAGE pathway analysis against Molecular Signatures Database (MSigDB). (B, E) Volcano plots of differentially expressed genes. Genes from IFN α/β (red), IFNγ (blue) and IRF transcription factor (green) pathways are marked. Cd207 (pink) is additionally marked in (B). (C, F) Log-transformed expression fold change for genes in the IFN α/β pathway. (G) Pathway similarity network built for the most enriched pathways (adjusted $p<0.005$) in CLE non-lesional skin determined by ranked GSEA (a complete list is in Table S5). Colors indicate network community clusters identified by the walktrap algorithm. Red borders indicate pathways that were also enriched in MRL/lpr mice (listed). (H) Comparison of gene expression changes from CLE (from B) and MRL/lpr mice (from E).

Figure 2

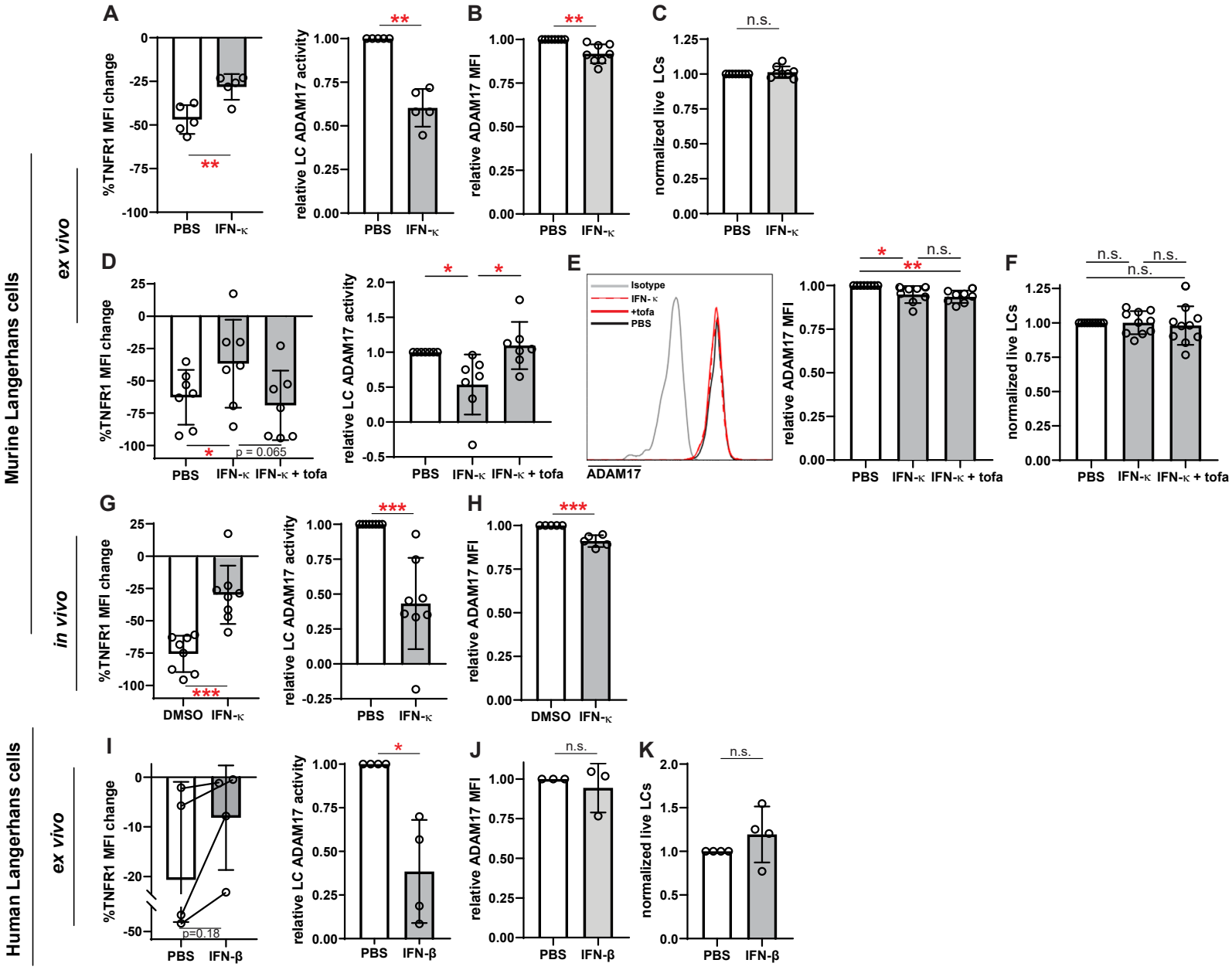

Figure 2. IFN-I can reduce LC ADAM17 sheddase activity. Prior to assay for UVR-induced LC ADAM17 sheddase activity, (A-C) epidermal cell suspensions from WT mice , (D-F) WT mice, and (G-H) suction blister epidermal cell suspensions from healthy human donors were treated with IFNκ, IFNκ +tofacitinib, or vehicle as indicated. For (D-F), treatments were applied topically to the ears for 16-20 hours. (A, D, G, I) LC ADAM17 sheddase activity as indicated by the extent of UVR-induced cell surface TNFR1 loss. (Left) %reduction in cell surface TNFR1 mean fluorescence intensity (MFI). (Right) LC ADAM17 activity is plotted as a function of the relative reduction in TNFR1 loss, normalized to the change in the vehicle condition. (B, E, H, J) Cell surface ADAM17 expression levels as indicated by MFI relative to that of MRL/+ isotype controls.(C, F, K) Relative numbers of LCs after indicated treatments. Each symbol represents (A-F, I-K) cells from a single mouse or healthy human donor across conditions or (G-H) a single mouse; bars represent average values and error bars are SD. n=4-10 per condition. *p<.05, **p<.01, ***p<.001, n.s.=not significant by unpaired t-test.

Figure 3

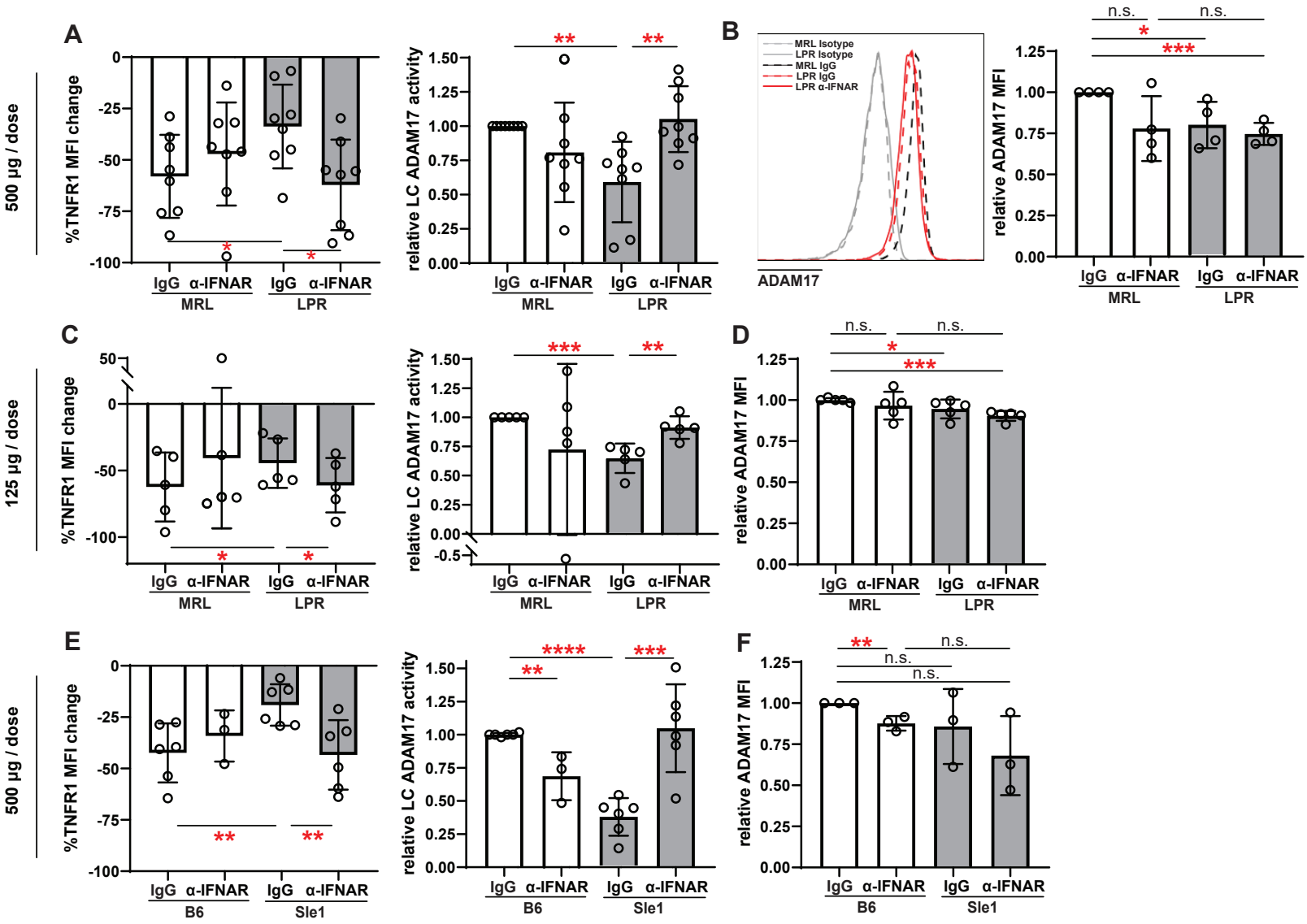

Figure 3. Anti-IFNAR1 restores LC ADAM17 activity in multiple lupus models. (A-D) MRL/+ and MRL/lpr mice and (E-F) B6 and B6.Sle1yaa mice were treated twice with anti-IFNAR1 or isotype control at indicated doses over 6 days. Epidermis was then collected and assayed for LC ADAM17 activity. (A, C, E) LC ADAM17 sheddase activity as indicated by the extent of UVR-induced cell surface TNFR1 loss. (Left) % reduction in cell surface TNFR1 mean fluorescence intensity (MFI). (Right) LC ADAM17 activity is plotted as a function of the relative reduction in TNFR1 loss, normalized to the change in MRL/+ isotype controls. (B, D, F) Cell surface ADAM17 expression levels as indicated by MFI relative to that of MRL/+ isotype controls. (A-F) Each symbol represents a mouse; bars represent average values and error bars are SD. n=8 (A), 4 (B), 5 (C-D), 6 (E), 3(F) per condition. *p<.05, **p<.01, n.s.=not significant by paired (A,C,E l(eft)) or unpaired t-test (A,C,E (right), B, D, F).

Figure 4

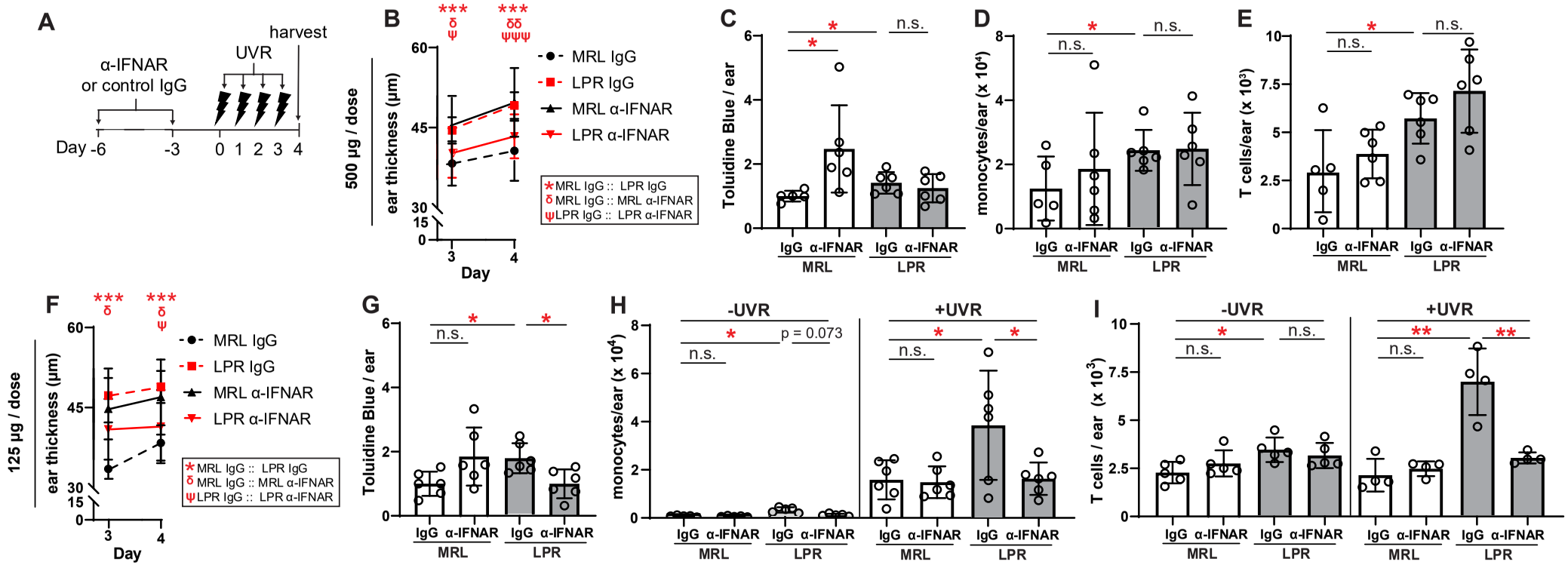

Figure 4. Anti-IFNAR reduces photosensitivity in MRL/lpr mice. (A-I) MRL/+ and MRL/lpr mice were treated twice with anti-IFNAR1 or isotype control over 6 days at indicated doses and then exposed to UVR daily for 4 doses prior to harvest of ear skin. (A) Schematic of experimental setup. (B, F) Ear thickness. (C, G) Epidermal permeability as indicated by toluidine blue retention. (D, H) Monocyte and (E, I) T cell numbers. (B, F) Each symbol represents the average value. (C-E,G-I) Each symbol represents one mouse and bars represent average values. (B-I) Error bars are SD and n=6 per condition. For (B, F), δ and ψ p<.05, δδ p<.01, *** and ψψψ p<.001, at indicated time points by unpaired t-test. For (C-E, G-I) *p<.05, **p<.01, n.s.=not significant by unpaired t-test.

Figure 5

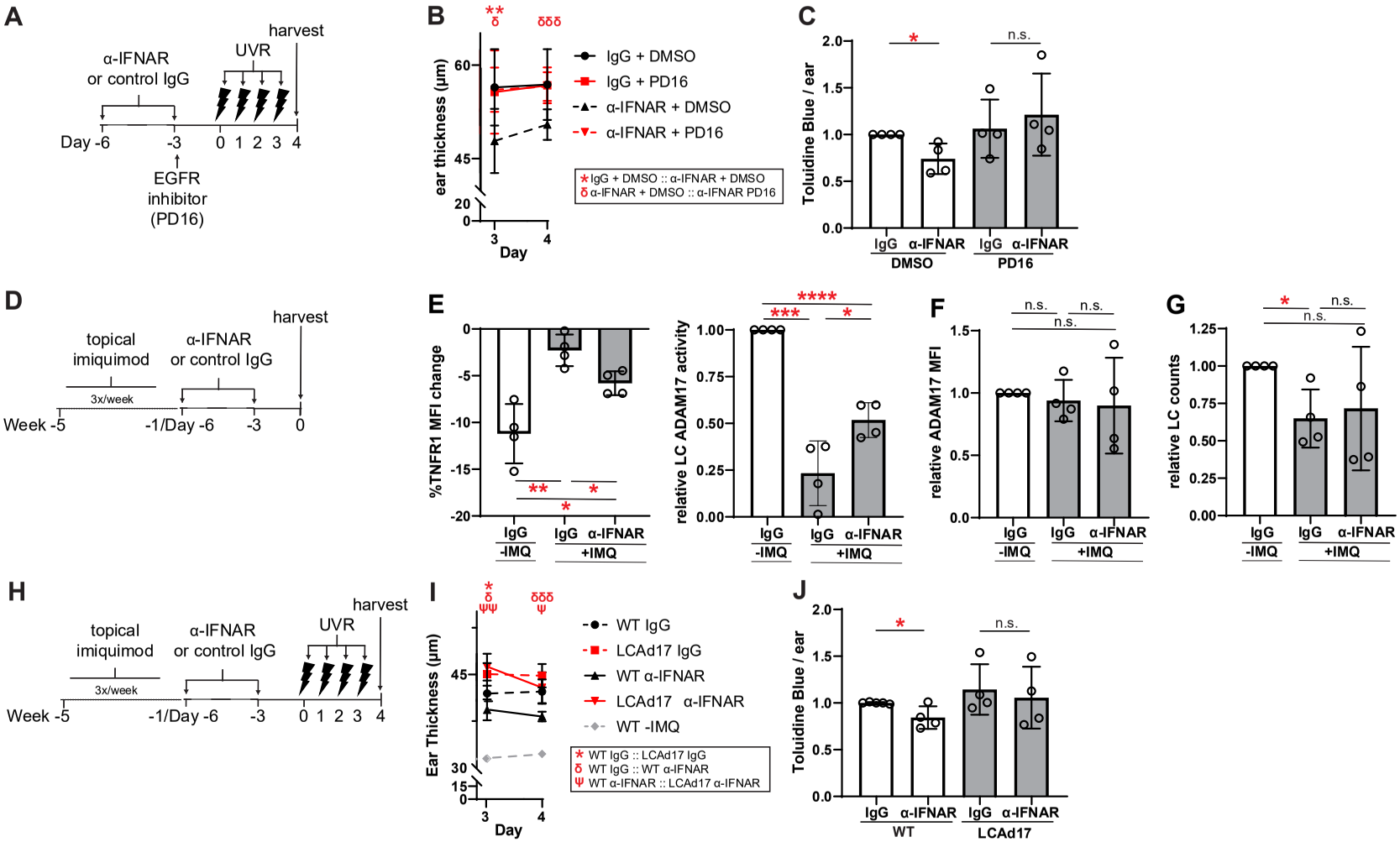

Figure 5. Reduction of photosensitivity by anti-IFNAR1 is dependent on EGFR and LC ADAM17. (A-C) MRL/+ and MRL/lpr mice who received anti-IFNAR1 or isotype control at 125ug/dose over 6 days were treated topically on ears with vehicle or the EGFR inhibitor PD168393 prior to UVR exposure and harvest. (A) Experimental setup. (B) Ear thickness. (C) Epidermal permeability as indicated by toluidine blue retention. (D-G) Wildtype mice were treated with imiquimod (IMQ) or vehicle for 4 weeks prior to anti-IFNAR1 or isotype control treatment and trunk skin was assessed for LC ADAM17 activity. (D) Experimental setup. (E) LC ADAM17 sheddase activity as indicated by the extent of UVR-induced cell surface TNFR1 loss. (Left) % reduction in cell surface TNFR1 mean fluorescence intensity (MFI). (Right) LC ADAM17 activity is plotted as a function of the relative reduction in TNFR1 loss, normalized to the change in vehicle-treated control. (F) Cell surface ADAM17 expression as indicated by MFI relative to that of vehicle-treated control. (H-J) LCAd17 and control mice received same treatment as in (D-G), exposed to UVR, and assessed for photosensitivity. (H) Experimental setup. (I) Ear thickness. (J) Epidermal permeability as indicated by toluidine blue retention. (B, I) Each symbol represents the average value. (C, E-G, J) Each symbol represents one mouse and bars represent average values. (B-C, E-G, I-J) Error bars are SD and n=4-5 per condition. (B, I), *, δ, ψ p<.05 and **p<.01,δδδ and ψψψ p<.001 at indicated time points by unpaired t-test. (C, E-G, J) *p<.05, ***p<.001, n.s.=not significant by unpaired t-test.

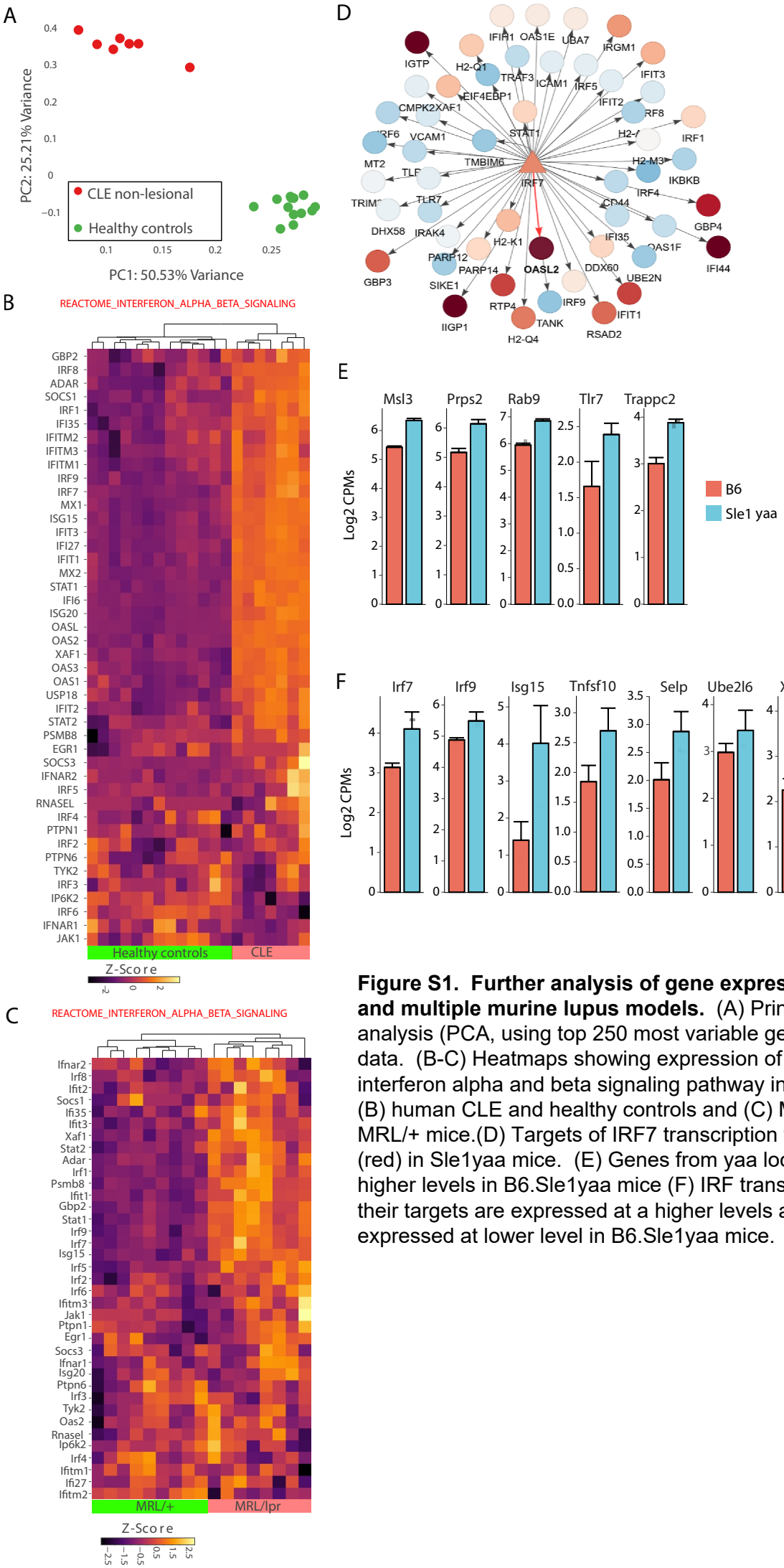

Figure S1. Further analysis of gene expression in human CLE and multiple murine lupus models. (A) Principal component analysis (PCA, using top 250 most variable genes) of microarray data. (B-C) Heatmaps showing expression of the genes of the interferon alpha and beta signaling pathway in non-lesional skin of (B) human CLE and healthy controls and (C) MRL/lpr and control MRL/+ mice.(D) Targets of IRF7 transcription factor upregulated (red) in Sle1yaa mice. (E) Genes from yaa locus are expressed at a higher levels in B6.Sle1yaa mice (F) IRF transcription factors and their targets are expressed at a higher levels and CD207 is expressed at lower level in B6.Sle1yaa mice.

Figure S1

Figure S2

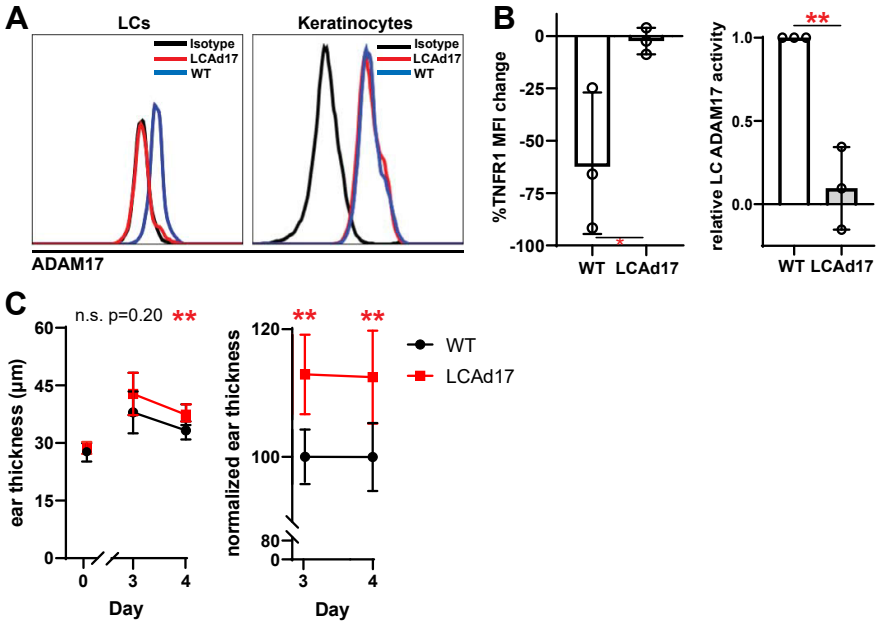

Figure S2. ADAM17 expression levels in LCAd17 mice, UVR-induced cell surface TNFR1 loss on LCs in mixed epidermal cell suspensions is dependent on LC ADAM17, and LCAd17 mice show UVR-induced ear swelling. (A-B) Epidermal cell suspensions from WT or LCAd17 mice were examined. (A) ADAM17 cell surface protein expression on LCs and keratinocytes. Representative of 3 experiments. (B) UVR-induced cell surface TNFR1 loss on LCs is dependent on LC ADAM17. (Left) % reduction in cell surface TNFR1 mean fluorescence intensity (MFI). (Right) LC ADAM17 activity is plotted as a function of the relative reduction in TNFR1 loss, normalized to the change in WT mice. (C) WT or LCAd17 ear thickness was examined at homeostasis or on days 3 and 4 after daily doses of 250J/m2 UVR on days 0-3. (Left) Eart thickness. (Right) Ear thickness normalized to WT day 3 values. (B) Each symbol represents 1 mouse. (C) Each symbol represents average of n=4-5 mice. Error b are SD. **p<.01 , n.s.=not significant by unpaired t-test.

Figure S3

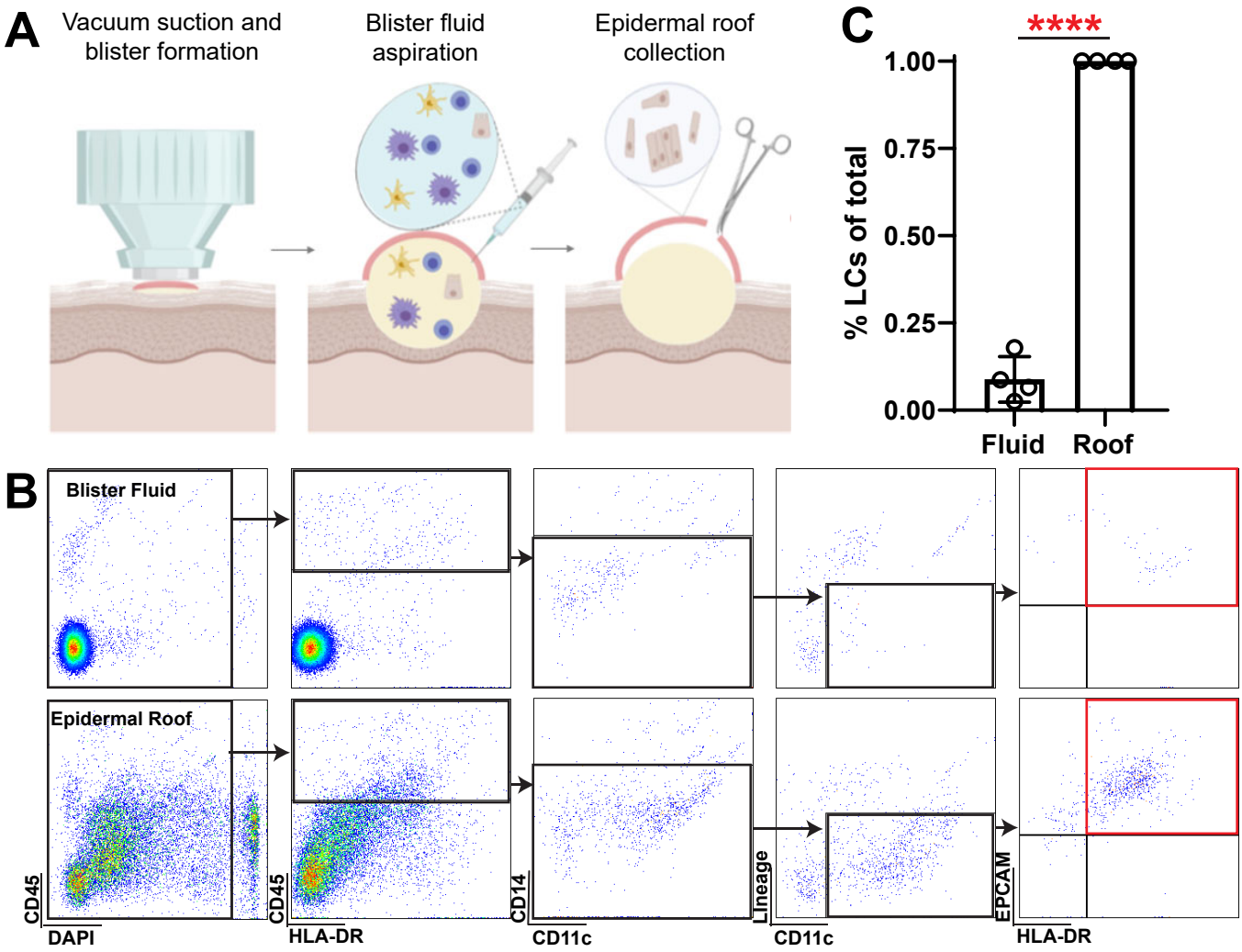

Figure S3. Langerhans cell yield and gating with suction blistering of human skin. (A) Schematic of suction blistering and sample collection. (B) Gating of Langerhans cells in blister fluid and in epidermal roof cell suspension. (C) Langerhans cell abundance in blister fluid and epidermal roof samples. Each symbol represents 1 healthy donor. ****p<.0001 unpaired t-test.